Kyaw, CT, Becker, AA, Sun, W, Effects of compositions of filler, binder and porosity on elastic and fracture properties of nuclear graphite**, Journal of Nuclear Materials**, Vol. 457 p. 42-47, 2015.

# Effects of compositions of filler, binder and porosity on elastic and fracture properties of nuclear graphite

**S.T. Kyaw*, W. Sun, A.A. Becker**

Faculty of Engineering, The University of Nottingham
University Park, Nottingham, NG7 2RD, UK

***Corresponding author email:** si.kyaw@nottingham.ac.uk
**Address: C03, ITRC building, University Park, University of Nottingham, NG7 2RD**
**Phone: +44-1159513811**

## Abstract

Physical mechanisms at different length scales have to be taken into account while predicting the overall failure of nuclear graphite structures of advanced gas cooled graphite reactors. In this paper, the effect of composition of meso graphite phases and porosity on the aggregate elastic properties is predicted using the Eshelby homogenisation method. Results indicate an overall decrease in elastic modulus with an increase in porosity. Subsequently, the moduli at different porosity levels are used to predict the critical strain energy release rates for crack propagation of graphite, and fracture behaviour is studied using compact tension and four point bending tests. Compared to flexural strength at zero porosity level, significant reduction in strength of up to 80% at 30% porosity level is observed. Evolution of flexural strength due to porosity is also compared against available experimental values of graphite from UK nuclear plants.

**Keywords:** Nuclear graphite, micromechanics, graphite phases, fracture mechanics

## 1 Introduction

Advanced gas-cooled reactors (AGR) within the UK are near the end of their safety life and currently significant research efforts have been invested to study whether the closure dates can be extended. Since AGRs are graphite-moderated, the damage mechanisms and subsequent fracture behaviour of graphite material need to be understood in order to estimate the safe lifetime of graphite structures.

Polycrystalline graphite used in the nuclear graphite industry is manufactured by mixing and baking a mixture of binder matrix and coke filler particles. Coal tar pitch or petroleum

pitch can be used as binder depending on the grade of graphite. The resultant heterogeneous material also has porosity (pore size varies from sub μm to hundreds of μm) and microscopic intra-crystal defects in the forms of microcracks [1]. As this type of graphite undergoes years of operation, the fast neutron damage and oxidation cause dimensional change in the crystals, material properties changes in the phases, and increase in total porosity. These changes can be studied at different scale ranges, from atomistic to mesoscopic scales. Linking these mechanistic multiscale effects to changes in the material properties is necessary. However, the homogenization of random multiscale mechanisms into a macroscopic structural analysis has proved to be challenging.

An attempt to link the mesoscopic and macroscopic scales is presented in this paper. Previous work [2] has shown the use of micromechanics to formulate the properties of aggregates composed of meso phases (binder and filler) and porosity within nuclear graphite. On this basis, a similar micromechanics-based homogenisation technique is applied and a further study of the effects of those phases on the fracture behaviour of nuclear graphite is also carried out. Evolution of flexural strength due to porosity is also compared against available experimental values of graphite from UK nuclear plants from the literature.

## 2 Micromechanics based model for effective elastic properties of nuclear graphite

### 2.1 Eshelby homogenisation method

It is challenging to take account of the effects of microstructures while analysing the failure of engineering components due to large difference in length scales. To avoid the complexity of modelling microstructural graphite phases implicitly using multi-scale models, a homogenisation technique is used to predict the elastic property of heterogeneous nuclear graphite in this paper. The homogenisation scheme applied here is based on Eshelby's method [3] and it is chosen over other continuum micromechanics methods since the method can be applied irrespective of shapes and numbers of phases. The method is briefly discussed here using a material composed of two homogeneous phases without porosity for simplicity, as in [4]. When the inclusion is taken out of the matrix and it is subjected to the eigenstrain ( $\varepsilon_{kl}^{*}$) or stress free strain, this eigenstrain would be cancelled by the elastic strain of the inclusion ( $\varepsilon_{kl}^{el}$) due to strain compatibility. The stress within the inclusion can be written as Eq (1) while stress and strain within the matrix are still zero. Once this inclusion is put back into its original place within the matrix, both matrix and inclusion surfaces will experience additional stress ( $\sigma_{ij}^{c}$) and strain ( $\varepsilon_{kl}^{c}$) for the constrained field of Green's function [4]. Due to

this additional stress, the stress within the inclusion can now be written as Eq (2). The term $\left(\varepsilon_{kl}^{c}-\varepsilon_{kl}^{*}\right)$ represents the elastic strain of the inclusion.

$$\sigma_{ij}=C_{ijkl}\varepsilon_{kl}^{*}=-C_{ijkl}\varepsilon_{kl}^{el}=-\sigma_{ij}^{*}\text{, where } \sigma_{ij}^{*} \text{ is eigenstress} \tag{1}$$

$$\sigma_{ij}=\sigma_{ij}^{c}-\sigma_{ij}^{*}=C_{ijkl}\left(\varepsilon_{kl}^{c}-\varepsilon_{kl}^{*}\right) \tag{2}$$

The above method can be extended to inhomogeneous inclusions with an external strain of ($\varepsilon_{kl}^{0}$) by assuming that the stress within the inclusion is identical for both homogenous and inhomogenous cases. In tensor form, it can be written as Eq (3). The constrained strain can be linked to the eigenstrain via an Eshelby tensor ($S_{ijkl}$), which is a fourth order tensor, as shown in Eq (4). The Eshelby tensor is dependent on the shape of the inclusions and for this study only spherical inclusions are considered for simplicity. For non-spherical inclusions, such as an ellipsoid shape, anisotropic Eshelby tensor is required and the material stiffness will be increased if the loading is applied along the major axis of the ellipsoid or vice versa.

$$C_{ijkl}\left(\varepsilon_{kl}^{c}+\varepsilon_{kl}^{c}-\varepsilon_{kl}^{*}\right)=C_{ijkl}^{m}\left(\varepsilon_{kl}^{c}+\varepsilon_{kl}^{0}\right)\text{, where } C_{ijkl}^{m} \text{ is the stiffness matrix of the inclusion} \tag{3}$$

$$\varepsilon_{ij}^{c}=S_{ijkl}\varepsilon_{kl}^{*} \tag{4}$$

**2.2 Formulation of elastic moduli of heterogeneous materials with spherical inclusions**

The Eshelby's homogenisation method was modified for the materials with more than one inclusion by Budiansky [5]. The procedure was also applied for heterogeneous coating material by Hermosilla [6] and it will be briefly described here. Assuming that the material is composed of N phases and the sum of volume fractions of those phases ($V_f^i$) is one for a volume conservation, the shear modulus (G) and the bulk modulus (K) of the aggregate can be linked to phases properties ($G^i$ and $K^i$) as shown in Eq (5) and (6).

$$\sum_{i=1}^{N}\frac{V_f^i}{1+\beta^t\left(\frac{G^i}{G}-1\right)}=1 \tag{5}$$

$$\sum_{i=1}^{N}\frac{V_f^i}{1+\beta^n\left(\frac{K^i}{K}-1\right)}=1 \tag{6}$$

$\beta^t$ and $\beta^n$ are linked to the aggregate Poisson's ratio as shown in Eq (7) and (8), and aggregate Possion's ratio can be expressed in terms of the bulk and shear moduli as shown in

Eq (9). For known elastic properties of N phases, Eq (5) to (9) can be solved simultaneously to obtain elastic properties of the whole media.

$$\beta^t = \frac{2(4-5\nu)}{15(1-\nu)} \tag{7}$$

$$\beta^n = \frac{(1+\nu)}{3(1-\nu)} \tag{8}$$

$$\nu = \frac{3K-2G}{6K+2G} \tag{9}$$

## 3 Application of Eshelby homogenisation method to elastic properties of graphite

To apply the Eshelby homogenisation method to the elastic properties of nuclear graphite, the properties of its constituent phases (filler and binder) are required. The elastic properties of the binder was taken from the nano-indentation test by Berre et al. [7]. The elastic modulus of coke filler was estimated using a zero porosity overall modulus and data from radiolytic oxidation experiments in [2] and the resultant value is taken for this analysis. Due to insufficient data, Poisson's ratio of aggregate graphite from [8] is taken as the value for both filler and binder. The material properties are listed in Table 1. The initial filler volume within quasi-isotropic graphite with spherical coke filler particles is 60% which was taken from X-ray tomography images performed by Berre et al. [2]. This volume is taken as constant for the current analysis and the porosity volume is increased from 0% to 30% with an increment of 5%.

**Table 1: Material properties for binder and filler of graphite**

| | **Binder** | **Filler** |
|---|---|---|
| E (GPa) | 15 [7] | 41[2] |
| v | 0.2 [8] | 0.2 [8] |

To compare the results from the Eshelby method to other independent results, three sets of data were chosen in which two sets are from simple models (Voigt and Knusden models) and the other set is from the experiments by Kelly et al. [9]. Voigt model uses a weight mean of phase volumetric proportions ($v_f^i$) to predict the aggregate properties as in Eq (10). The model is only applicable to axial loading cases. Knusden model can be expressed in terms of the initial elastic modulus with zero porosity ($E_0$) and porosity volumetric ratio (P) as shown

in Eq (11) where b is an empirical parameter, which depends on the aspect ratio of the pore (a/c) as shown in Eq (12).

$$E = \sum_{i=1}^{N} V_f^i E^i \tag{10}$$

$$E = E_0 \, e^{(-b \times P)} \tag{11}$$

$$b = 1 + 0.594 \times (a/c) \tag{12}$$

The moduli of graphite based on porosity proportion for all three models are plotted in Fig. 1. For Knusden's model three aspect ratios of porosity, based on different values of b, were also taken into account. An aspect ratio of 1 is similar to the Eshelby model for the current case. The other aspect ratios are calculated with an empirical b value of 3.6 by Kelly et al. [9] and 2.8 by Brocklehurst et al. [10]. Overall, the Voigt model predicts the highest value of the moduli while results from the Eshelby model closely follow the values predicted by Knusden law with the spherical inclusion. However, experiments predict much lower moduli. Moreover, the changes in elastic modulus from experiments also show a highly non-linear relationship whereas only slight non linearity was observed from the predictions by the Eshelby model. This indicates the need for implementing variable aspect ratios within the Eshelby model in the future.

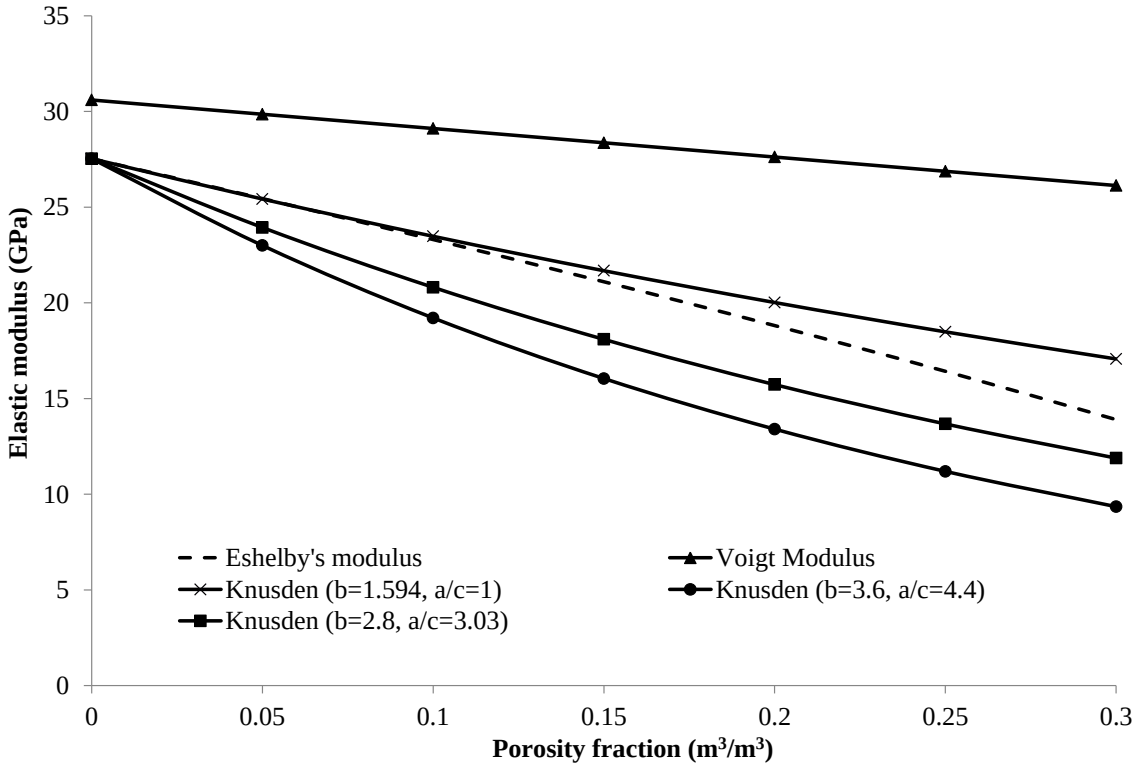

**Fig. 1: Modulus from Eshelby's homogenisation method for aggregate modulus of graphite compared to Knusden law with different ratio of 'b' and to Voigt modulus**

## 4 Fracture analysis of nuclear graphite

### 4.1 Effects of porosity and size of specimen on fracture strength

The strength of the graphite, like other quasi-brittle materials, is highly dependent on the size of the specimen used for testing [11, 12]. It is also common to have higher strength as the volume of the specimen is increased for quasi-brittle materials[12, 13]. This is because individual graphite features (size, shape and distribution of filler and binder phases and pores) influence the initiation and propagation of cracks. Moreover, porosity observed within nuclear graphite also affects its strength. Porosity can be observed both as closed pores due to shrinkage during the calcination stage and as open pores within the binder region due to gas evolution[14]. It has been shown that porosity volume within the binder matrix is increased due to radiolytic oxidation [15] and this could reduce the overall strength of the graphite [11]. In this paper, only the effect given by variations in overall volume proportions of pores and phases on overall strength is analysed. However, the effects by size, shape and distribution of both pores and phases on strength are not considered although they are shown to affect the strength of graphite [11].

### 4.2 Geometry and boundary conditions of finite element models for fracture analysis

To analyse the fracture behaviour of graphite with various porosity and phase proportions, two different specimens were used. They are a compact tension (CT) specimen and a four-point bending specimen. These types of specimen are chosen due to wide availability of experimental data for both virgin and irradiated graphite in the literature [16-19]. The geometry and boundary conditions for both specimens are shown in Fig. 2; B is the specimen thickness and I represents the initial crack length. Initial cracks are placed at the position where maximum damage is expected from the simulation of an initially damage free model. The full geometry is required to simulate compact tension test as it is to be used with extended finite element analysis (XFEM) which will be discussed in detail in the next section. Both tests are displacement controlled and a displacement of D is applied at the load points as shown in Fig. 2.

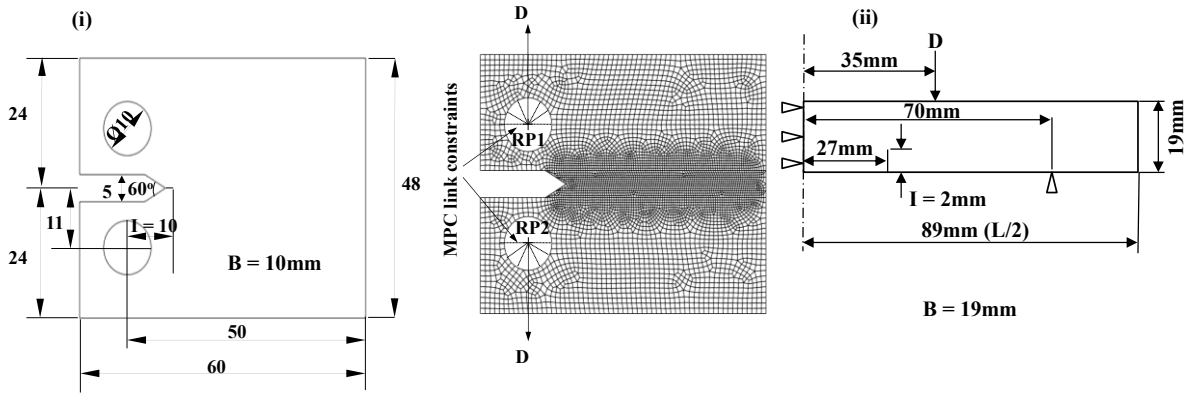


**Fig. 2: Geometry and boundary conditions of (i) compact tension specimen and (ii) four-point bending specimen**

### 4.3 Cohesive surface based coupled XFEM fracture model

Fig. 3 (i) shows the possible defects around the crack tip of graphite during the crack propagation. There can be micro-voids and uncracked bridging regions. The relationship between the crack opening displacement and the traction stresses across the crack surfaces can be modelled by using cohesive damage model (CDM), and Fig. 3 (ii) shows a simple bilinear CDM. Initially, the crack opening will be elastic until the opening reaches $u^i$ as shown in Fig. 3 (ii). Afterwards, damage initiates and traction stress decreases as the crack opens. If unloading and reloading occur the stiffness of the crack opening is reduced from the initial stiffness k to k (1-D). D is the damage parameter which is related to crack opening (u) as shown in Eq (13). The area under the traction/separation curve of Fig. 3 (ii) represents the critical energy used for crack propagation and it is usually measured empirically. A similar model has been used by others for failure predictions of nuclear graphite [20, 21].

$$D = \frac{u^*\left(u - u^i\right)}{u\left(u^* - u^i\right)} \tag{13}$$

For graphite, the fracture energy of the crack is found to be increased [19, 22] as the crack propagates through defects as shown in Fig. 3 (iii). The length of crack before the energy becomes stable is known as grain bridging length. Work is in progress [23] to use a trilinear cohesive damage model from [24] to model this type of behaviour. For the current study, a bilinear CDM is used. In this work the material is assumed to be elastic until the peak load and post peak load strain softening behaviour is modelled. Alternatively, work has also been

presented in the literature based on plastic hardening with isotropic damage mechanics in [25].

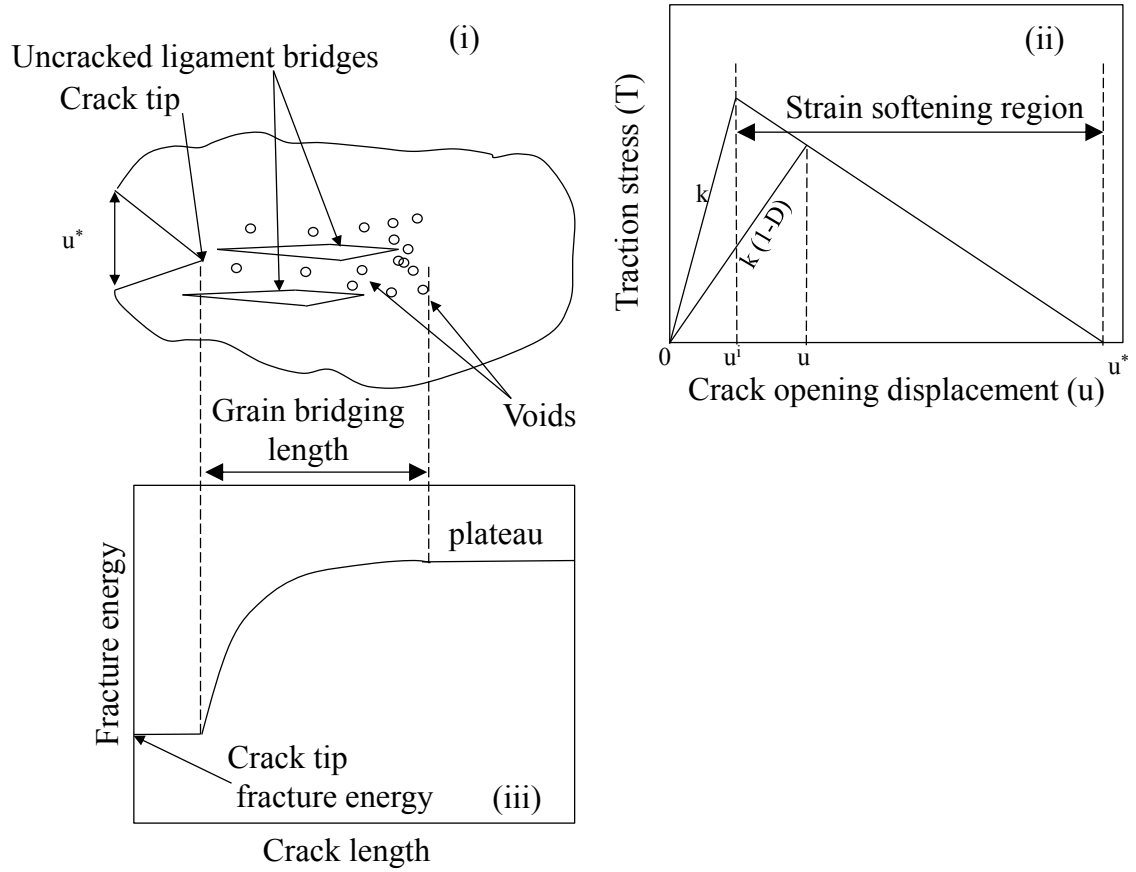


**Fig. 3: (i) Possible defects around the crack tip for graphite (ii) CDM using bilinear law to represent the relationship between traction stress against crack opening displacement (u) (iii) increase in fracture energy as the crack goes through ligaments and voids**

Using CDM alone will require a priori initial crack and crack propagation direction during the processing stage. To avoid this limitation, XFEM crack initiation and propagation criteria are used in conjunction with CDM. For initiation, the XFEM will add enrichment to the degrees of freedom of elements of FE model once the damage factor (f) exceeds unity. This damage factor can be defined based on critical stress or critical crack separation. It can also be used for mixed mode crack initiation. For our analysis, a nominal stress criterion is applied and the crack is assumed to propagate perpendicularly to the direction of the maximum nominal stress. For simplicity, only Mode I damage initiation is defined for the current study and the crack will propagate in a perpendicular direction to the nominal stress direction.

### 4.4 Material properties for damage model

Assuming the porosity within the graphite is the result of oxidation of binder phase alone and there is no change in the proportion of filler particles, a relationship between the fracture parameters and the porosity volume fraction is required. To use the cohesive/XFEM model for fracture, the critical stress for damage initiation and the fracture toughness ($K_C$) to calculate critical energy for damage propagation are necessary. An empirical relationship between the tensile strength and porosity given by Brocklehurst et al.[10] is taken for the failure stress evolution. A simple linear relationship between fracture toughness and porosity is used based on the assumption that the work of fracture is reduced based on area reduction [26]. For plane stress problems, the critical strain energy release rate (U) can be calculated using Eq (14).

$$U = \frac{{K_C}^2}{E} = \frac{\left(K_C^0(1-P)\right)^2}{E} \tag{14}$$

where $K_C^0$ is the initial fracture toughness. Elastic moduli for graphite at different porosity level are calculated from Eshelby homogenisation method. Initial fracture stress of 14MPa and strain energy release rate of 250 J/m$^2$ are taken from virgin graphite data [19]. Finally, failure stress and critical strain energy release rate against porosity can be plotted as shown in Fig. 4.

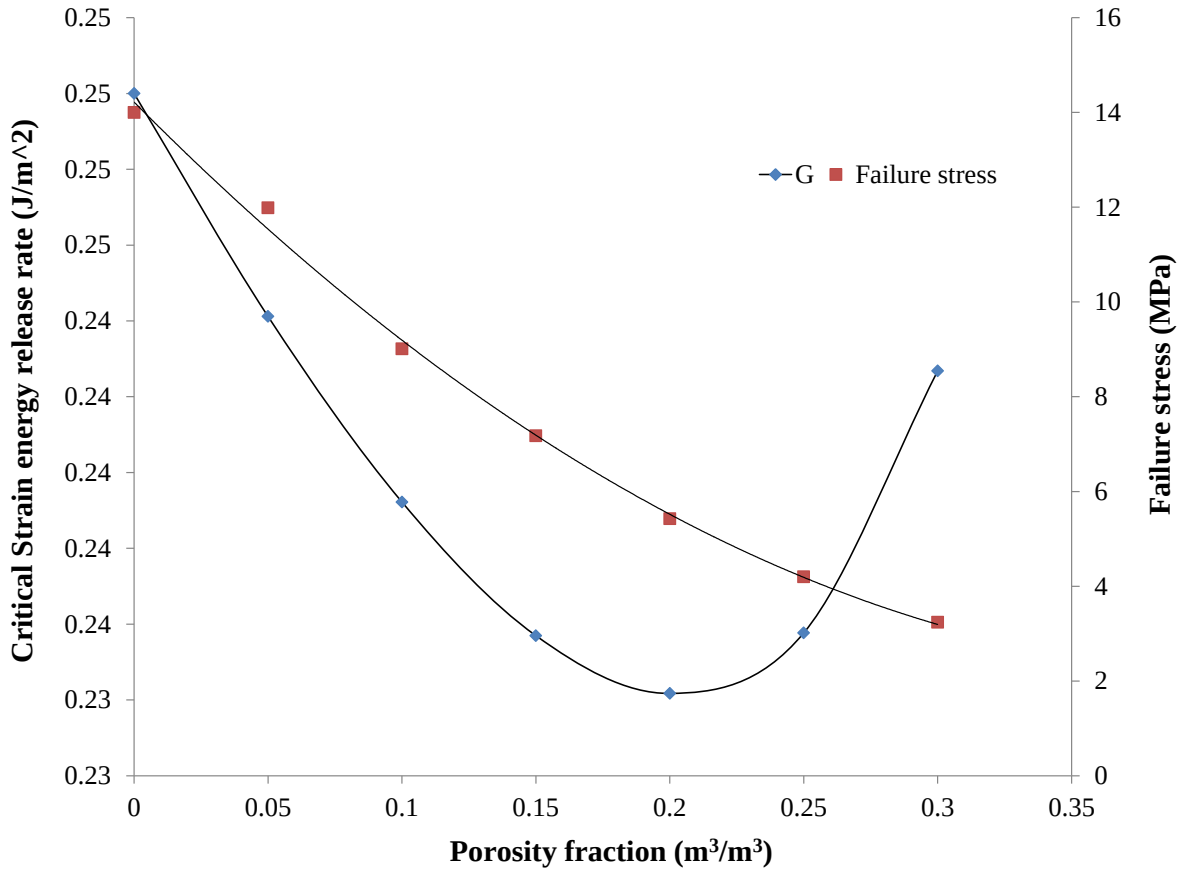


**Fig. 4: Failure stress and strain energy release rate against porosity volume fraction of graphite**

## 5 Results and discussion

From FE simulations for the CT and four-point bending tests with varying porosity levels, the reaction forces vs displacement plots for both tests were obtained and plotted in Fig. 5 and Fig. 6. In general, both tests show an initial linear region with its slope decreasing with porosity mimicking the decrease in elastic modulus due to porosity. Ratios of peak reaction forces at different porosity levels to porosity-free peak force for the CT and the four-point bending test specimens are plotted against porosity fraction as shown in Fig. 7. It shows that the peak reaction force (F) after which the material shows a softening behaviour decreases with porosity. The decrease in the critical tensile stress with increasing porosity has also been shown by the uniaxial tensile test simulation in [2] using the model reproduced from the actual tomographic images of graphite. However, there is no experimental test within the literature to verify this softening behaviour due to porosity. Nevertheless, the current observation proposes that crack initiation will occur at lower stress level as the graphite becomes more porous.

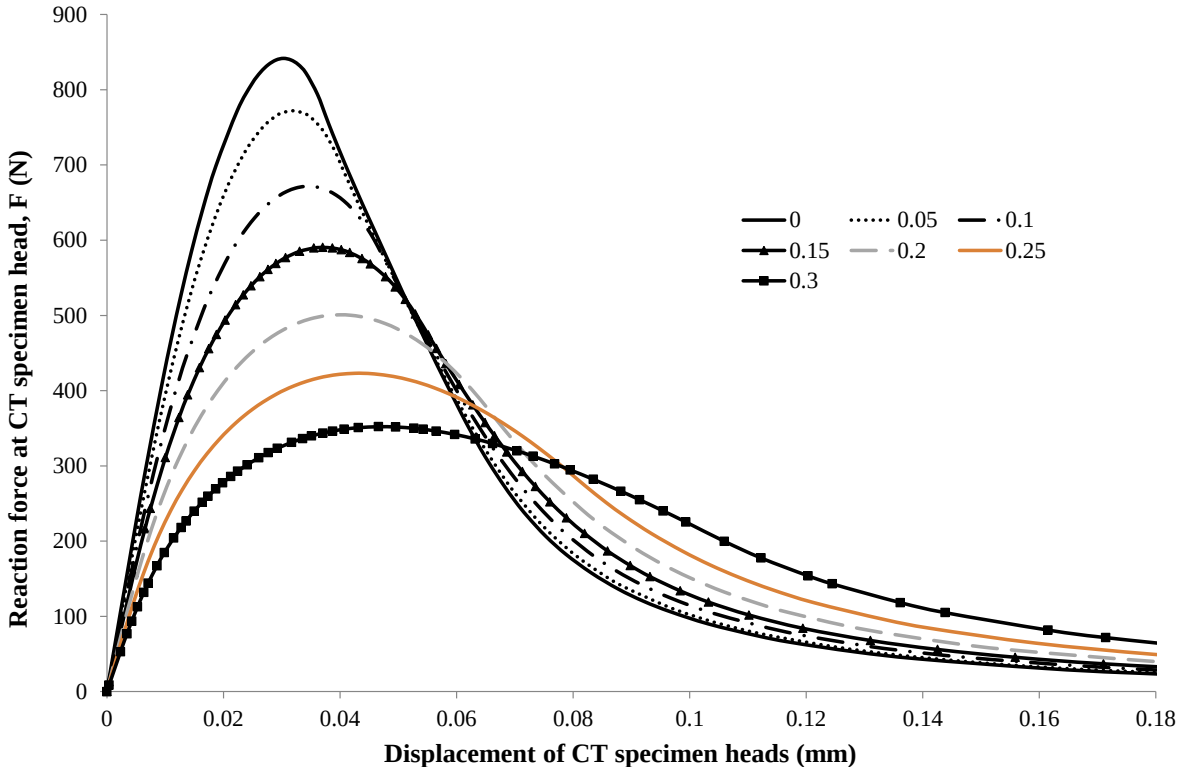


**Fig. 5: Force-displacement plot of CT test simulation at different porosity levels**

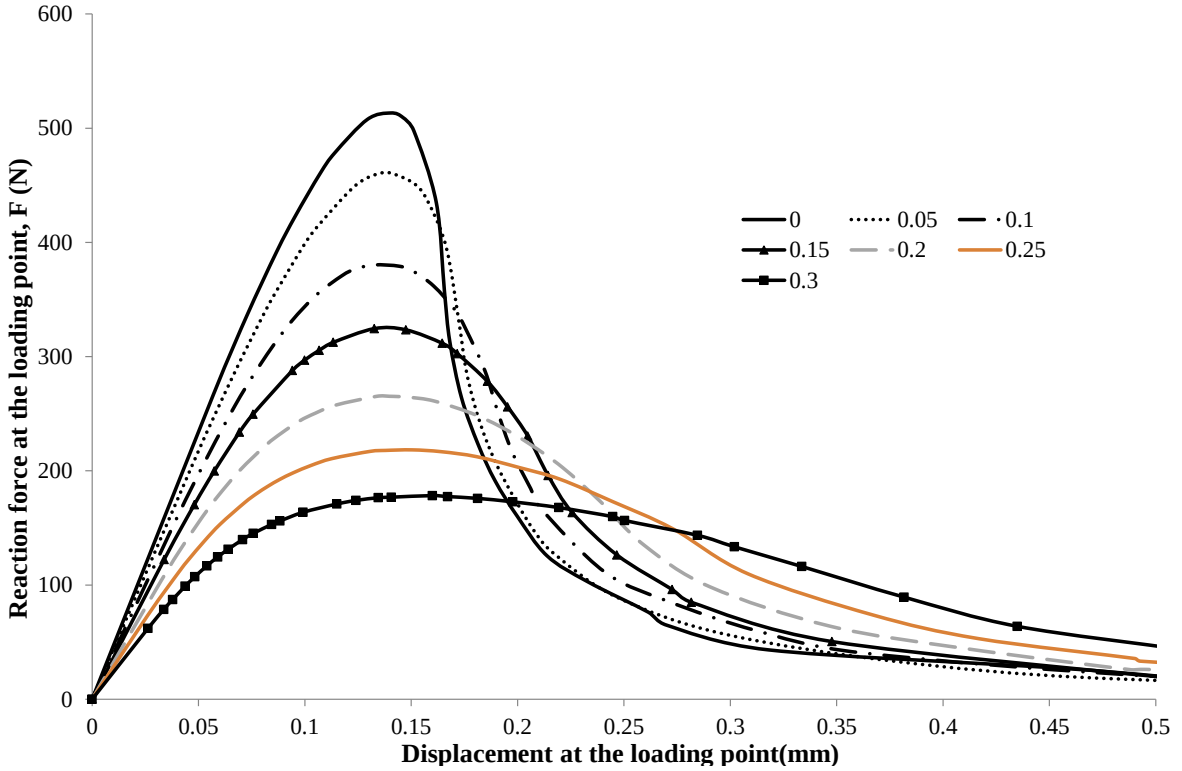


**Fig. 6: Force-displacement plot of four point bending test simulation at different porosity levels**

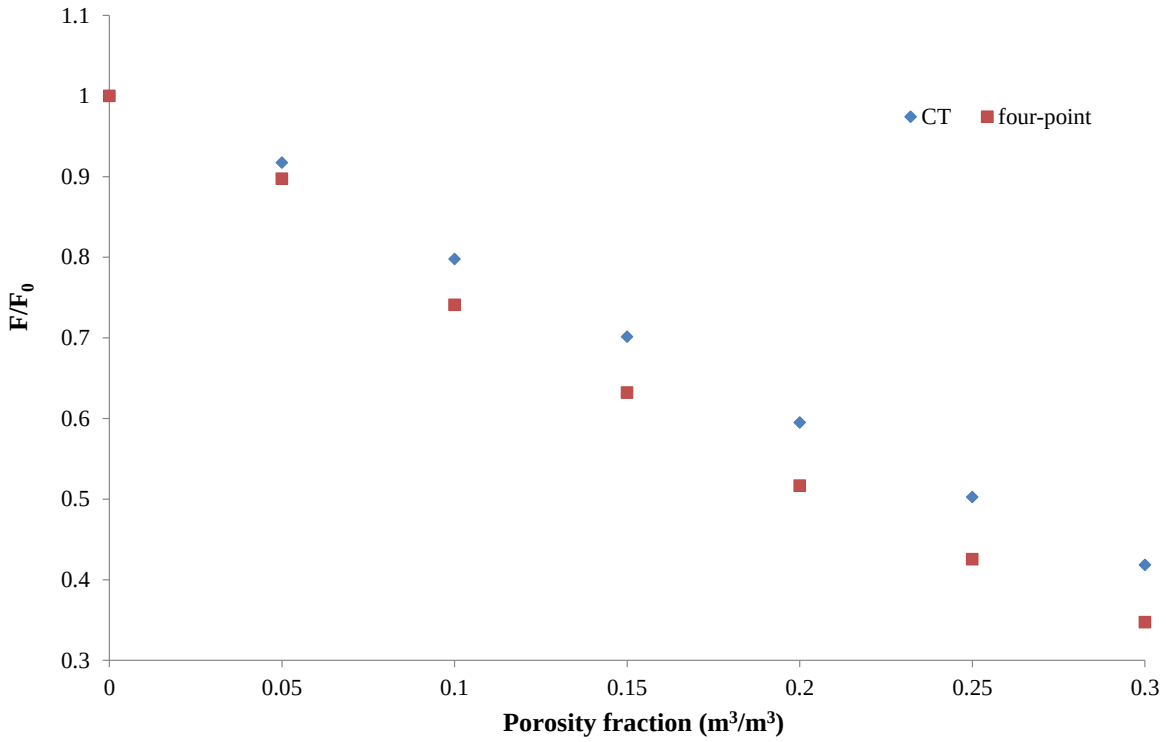


**Fig. 7: Maximum reaction forces normalised by initial reaction force at respective loading point for CT and four point bending tests at different porosity levels**

Flexural or bending strength is another important mechanical parameter that can be studied from four point bending simulations. To calculate bending strength of the four point bending specimen, the applied force, at which the onset of stable crack growth occurs, is required. In this case, the maximum reaction force, as plotted in Fig. 7, is taken as the critical force for the onset of crack growth. Although the initial crack within the specimen will reduce both reaction force and flexural strength, the effect will imply to all simulation similarly and the effect of porosity on flexural strength can still be observed. Resultant flexural strengths (S) normalised to the respective initial values at zero porosity level ($S_0$) are plotted in Fig. 8. Compared to the tensile strength evolution against porosity, the rate of decrease in flexural strength with an increasing porosity is lower. Note that $S/S_0$ in Fig. 8 represents both tensile and flexural strength ratios.

The flexural strengths from four point bending simulation are also compared against available graphite strength data from different UK nuclear stations [16]. A regression line of the experimental data is used for the purpose of comparison while the variability of 10MPa is expected for experimental strength data. The variability could originate from differences in distribution and shape of graphite phases among graphite specimens. The strength ratio from the FE analysis agrees well with G3 HNB graphite material and a linear relationship between

experimental and FE solutions can be observed as plotted in Fig. 9. The numerical results also follow closely to the trend of G2 HPB material mainly due to its similarity to G3 HNB graphite. It is noteworthy that the difference in the size of experimental specimen and specimen size used for simulation is not taken account when comparing the strength data in Fig. 9. Although the size effect has been mentioned in [12], only experimental strength ratios at different porosity levels normalised by virgin graphite strength are compared to numerical results in this paper. For quantitative comparison of strength values further sensitivity analysis with different sizes of specimen is required.

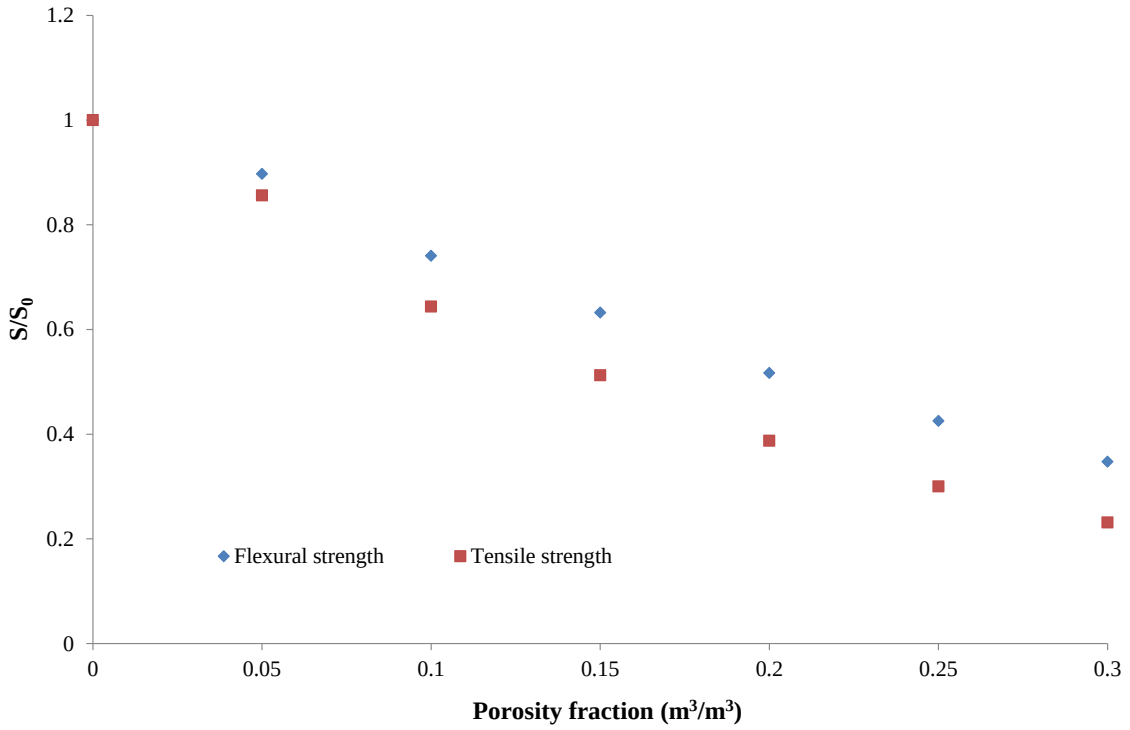


**Fig. 8: Flexural strength compared to tensile strength results from four point bending tests with a range of porosity fraction**

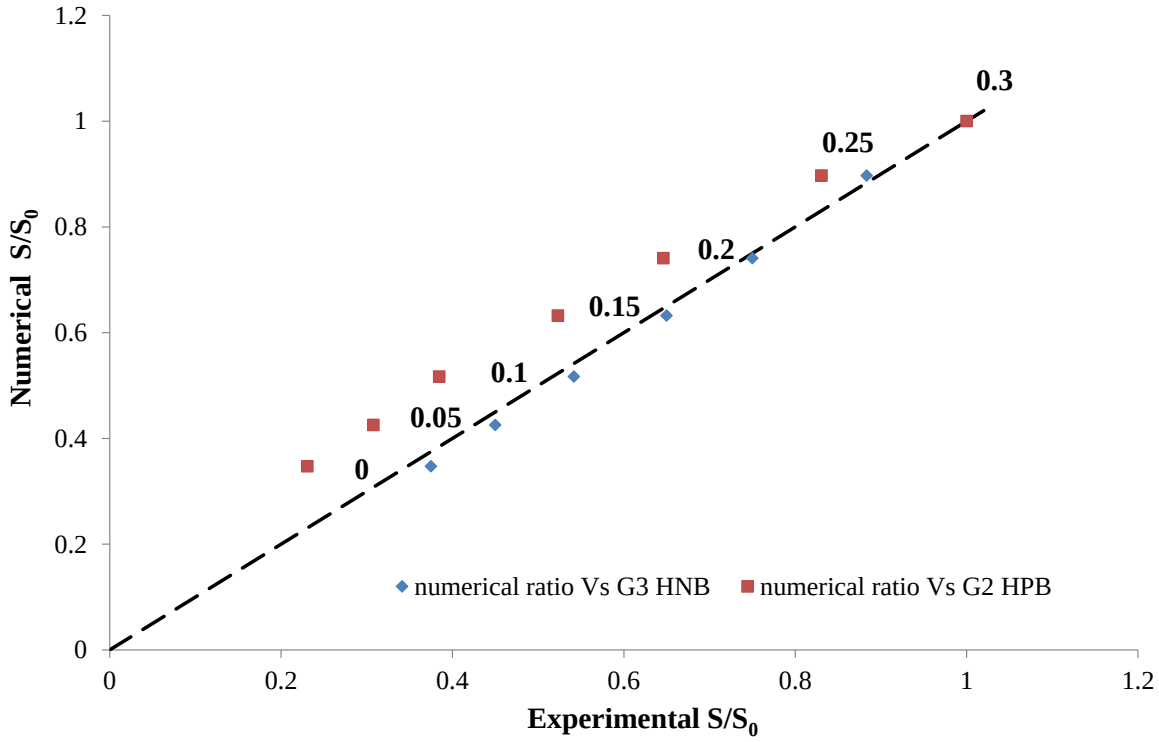


**Fig. 9: Flexural strength ratios from four point bending test simulation and from experiments [16] with a range of porosity fraction**

## 6 Conclusions and future work

The paper presents the use of a micromechanics-based homogenisation technique as a tool to observe the effects of the composition of graphite meso phases and porosity on the overall elastic properties. The technique can also be applied to calculate the elastic properties of representative volume of graphite bricks used in industry considering different compositions of phases at different locations in the bricks. The resultant elastic modulus was also used to calculate the critical strain energy release rate for fracture mechanics analysis. Subsequently, the material data are used to simulate the CT and the four point bending tests. From these studies, a reduction in material strength before the onset of crack growth can be observed. Moreover, resultant changes in flexural strength due to porosity level from the four point bending test simulation are found to be within ± 7% of the experimental results of graphite from G3HNB plant while the trend in degradation of flexural strength is similar to the one by G2HPB graphite [16]. Resultant formulations of elastic modulus and fracture properties of graphite based on porosity level from the current analysis can be implemented within the failure analysis of the nuclear graphite structures, which makes use of CDM [21, 27, 28]. Cracks are expected to initiate quicker as the moderator brick becomes more porous from

oxidation since the strength of graphite is predicted to be reduced with increasing porosity level.

In the current study, the effect of irradiation is not taken into account. Neutron radiation can cause changes in the material properties of the filler and binder phases, and these changes should be coupled into the Eshelby homogenisation method in future analyses. For this study, it is assumed that oxidation reduces only the proportion of binder phase whereas the proportion of filler phase is fixed. Radiolytic oxidation, when irradiation is considered within the model, will oxidise the graphite more uniformly and this effect on binder/filler volumetric ratio needs to be investigated further. Moreover, investigating into the effects of different shapes of pore on the Eshelby tensor and the resultant elastic modulus will be carried out. The work presented in the current paper will also serve as a basis for complex two-scale damage models which incorporate the relationship between non elastic strains at mesoscopic and macroscopic levels into the modelling of the damage initiation within quasi brittle nuclear graphite.

**Acknowledgement**

The authors would like to acknowledge the financial support of EPSRC through a joint project "Long Term Materials Behaviour and Chemistry - Fundamentals of Current and Future Uses of Nuclear Graphite" (EP/1002707/1).

**References**

[1] A.N. Jones, G.N. Hall, M. Joyce, A. Hodgkins, K. Wen, T.J. Marrow, et al. Microstructural characterisation of nuclear grade graphite. J. Nucl. Mater. 381 (2008) 152-7.
[2] C. Berre, P.M. Mummery, B.J. Marsden, T. Mori, P.J. Withers. Application of a micromechanics model to the overall properties of heterogeneous graphite. J. Nucl. Mater. 381 (2008) 124-8.
[3] J.D. Eshelby. The determination of the elastic field of an ellipsoidal inclusion, and related problems. Proc. R. Soc. A. 241 (1957) 376-96.
[4] C. Weinberger, W. Cai, D. Barnett. Lecture Notes - Elasticity of Microscopic Structures. (2005).
[5] B. Budiansky. On the elastic moduli of some heterogeneous materials. J. Mechs. Phys. Solids. 13 (1965) 223-7.
[6] U. Hermosilla. Mechanical modelling of thermal barrier coatings at high temperatures. University of Nottingham. (Thesis (PhD), 2008).
[7] C. Berre, S.L. Fok, B.J. Marsden, L. Babout, A. Hodgkins, T.J. Marrow, et al. Numerical modelling of the effects of porosity changes on the mechanical properties of nuclear graphite. J. Nucl. Mater. 352 (2006) 1-5.

[8] D.K.L. Tsang, B.J. Marsden. The development of a stress analysis code for nuclear graphite components in gas-cooled reactors. J of Nucl Mater. 350 (2006) 208-20.
[9] B.T. Kelly, P.A.V. Johnson, P. Schofield, J.E. Brocklehurst, M. Birch. UKAEA NORTHERN DIVISION STUDIES OF THE RADIOLYTIC OXIDATION OF GRAPHITE IN CARBON-DIOXIDE. Carbon. 21 (1983) 441-9.
[10] J.E. Brocklehurst, R.W. Adam. Mechanical tests on graphite with simulated radiolytic oxidation gradients. UKAEA report, ND-R-853(S). (1983).
[11] A. Hodgkins, T. Marrow, M. Wootton, R. Moskovic, P. Flewitt. Fracture behaviour of radiolytically oxidised reactor core graphites: a view. MATER SCI TECH 26 (2010) 899-907.
[12] H. Li, J. Li, G. Singh, A. Fok. Fracture behavior of nuclear graphite NBG-18. Carbon. 60 (2013) 46-56.
[13] Z.P. Bazant. Size effect on structural strength: a review. Arch. Appl. Mech. 69 (1999) 703-25.
[14] 'Nuclear graphite production'. Nuclear Eng. (1957) 175-8.
[15] I.A. Vatter. Oldbury reactor 2 2005 installed sets - phase 3, Measurements. Part 3. Flexural tests - fractography. British Nuclear Group/Report MEN/ESTD/OLA/REP/0058/07, British Nuclear Group. (2007).
[16] E.D. Eason, G.N. Hall, B.J. Marsden, G.B. Heys. Models of bending strength for Gilsocarbon graphites irradiated in inert and oxidising environments. J. Nucl. Mater. Volume 436 (2013) p. 208-16.
[17] O. Pierre, B.N. Gareth, M. Brian. Controlled crack growth in an oxidized nuclear grade graphite. J. Phys. D: Appl. Phys. 37 (2004) 3192.
[18] S. Fazluddin. Crack Growth Resistance in Nuclear Graphite. PhD thesis (The University of Leeds). (2002).
[19] P. Ouagne, G.B. Neighbour, B. McEnaney. Crack growth resistance in nuclear graphites. J. Phys. D: Appl. Phys. 35 (2002) 927.
[20] Z. Zou, S.L. Fok, S.O. Oyadiji, B.J. Marsden. Failure predictions for nuclear graphite using a continuum damage mechanics model. J. Nucl. Mater. 324 (2004) 116-24.
[21] Z. Zou, S.L. Fok, B.J. Marsden, S.O. Oyadiji. Numerical simulation of strength test on graphite moderator bricks using a continuum damage mechanics model. Eng Fract Mech. 73 (2006) 318-30.
[22] M. Sakai, J.-I. Yoshimura, Y. Goto, M. Inagaki. R-Curve Behavior of a Polycrystalline Graphite: Microcracking and Grain Bridging in the Wake Region. J of the Am Ceram Soc. 71 (1988) 609-16.
[23] S.T. Kyaw, A.A. Becker, W. Sun. An overview of cohesive damage models for simulating crack growth energy of nuclear graphite. The 4th EDF Energy Nuclear Graphite Symposium. Engineering Challenges Associated with the Life of Graphite Reactor Cores, Nottingham, UK. (2014).
[24] C.G. Dávila, C.A. Rose, P.P. Camanho. A procedure for superposing linear cohesive laws to represent multiple damage mechanisms in the fracture of composites. Int J Fracture. 158 (2009) 211-23.
[25] T. Becker, J. Marrow. Modelling Damage in Nuclear Graphite. 13th International Conference on Fracture ,Beijing, China. (June 16-21, 2013).
[26] Buch.J.D. Mechanical Behavior Model for Graphites. Properties Related to Fracture Toughness By W. R. Warke, American Society for Testing, Materials., Umberto Colombo (1976).
[27] S. Kyaw, D. Tanner, A. Becker, W. Sun, D. Tsang. Modelling crack growth within graphite bricks due to irradiation and radiolytic oxidation. 20th European Conference on Fracture, Trondheim, Norway. (2014).

[28] P. Martinuzzi, L. Pellet. Modelling Crack Propagation in AGR Graphite Bricks in Code_Aster Using the eXtended Finite Element Method. 4th International Conference on Crack Paths, Gaeta, Italy. (2012) pp 831-8.